Single-Phase Current-Source Grid-Connected Inverter Based on Boundary Voltage Control

Liqiao Wang, Zhaozhao Tang, Xiaoshan Xing, and Zong Li

***Abstract*—A boundary voltage control (BVC) strategy suitable for single-phase current-source inverters has been proposed to achieve zero current switching (ZCS) by dynamically adjusting the resonant capacitor voltage, and this control strategy has low requirements for dc side current ripple, which can effectively reduce the dc side inductance value. Therefore, this control method can reduce circuit losses and decrease the size of the inverter. In this article, the working principle and conditions for achieving ZCS are analyzed by combining BVC and bipolar modulation strategy. Based on the principle of area equivalence, a quantitative model of dc side inductor current and output current is established, revealing the mechanism of the impact of second harmonic current ripple on output harmonics. The optimization design criteria for dc side inductance parameters are derived, and the reasons for the decrease in inductance value are analyzed. On this basis, a three loop grid-connected control strategy based on BVC is proposed. Finally, based on theoretical analysis, simulation and experimental research are conducted. The simulation and experimental results have verified the feasibility of the proposed BVC strategy.**

***Index Terms*—Inverter, lightweight, photovoltaic power generation, zero current switching (ZCS).**

I. Introduction

THE development of renewable energy is an important measure to address the energy crisis and environmental pollution [1]. Photovoltaic power generation has received the most attention in the application of renewable energy. Photovoltaic inverter is the most critical component in the photovoltaic power generation system [2], [3]. According to the energy storage components on the dc side, inverters can be divided into voltage-source inverters (VSI) and current-source inverters (CSI). The voltage of photovoltaic modules is usually lower than the grid voltage, which requires photovoltaic inverters to have step up capability. VSI does not have the ability to step up voltage. Therefore, a step-up dc converter is usually added in the front stage. CSI has inherent boosting capability, making it more suitable for applications in photovoltaic systems. And CSI does not require short-circuit protection or electrolytic capacitors, so its reliability and lifespan have been improved [4], [5]. In fact, from the perspective of photovoltaic systems, there are also some potential benefits. The dc side of CSI is an inductor, which ensures the continuity of the dc side current and helps achieve maximum power tracking of the photovoltaic system. In addition, the current of CSI flows unidirectional, theoretically avoiding the reverse flow of dc side current, without the need to add additional diodes.

However, CSI also have some limitations that restrict their application in medium and small power systems. In order to achieve stable input current, a large inductor is usually connected in series on the dc side. This not only increases the size and cost of the inverter but also reduces its efficiency. Therefore, the lightweighting of dc side inductance is a key issue that CSI urgently needs to address [6].

There are two methods to make the dc side inductance lightweight. The first method is to improve the inverter topology. In [7], a decoupling circuit is proposed, which is connected in series on the dc side, reducing ripple power by adjusting the buffer capacitor voltage in real time. A decoupling circuit that shares a switch between an inverter and a decoupling circuit is proposed in [8] and [9], which can transfer the pulsating power on the dc side to the capacitor of the decoupling circuit.

Another method is the improvement of the modulation strategy. The conventional sinusoidal pulse width modulation (SPWM) modulation follows the principle of area equivalence. In theory, it requires a ripple free dc side current. However, reducing the dc side inductance will increase the ripple of the dc side current. According to the principle of area equivalence, this can also lead to distortion of the ac side current. To solve this problem, a nonlinear modulation strategy is proposed in [10] to reduce the dc side inductance, but this method is more complex to control and does not provide a closed-loop control scheme. In [4], a nonlinear modulation strategy based on the principle of area equivalence is proposed. This method adjusts the modulation wave or carrier wave in real-time to ensure that the current impulse follows the sinusoidal variation. This method reduces the impact of dc side inductor current ripple on grid current. However, this method involves division operations, which result in relatively complex calculations.

The above methods are improvements to the fixed frequency SPWM modulation technology, and their switching actions strictly follow the principle of area equivalence. The ripple on

Received 21 March 2025; revised 24 May 2025, 19 July 2025, and 20 August 2025; accepted 28 August 2025. Date of publication 1 September 2025; date of current version 22 October 2025. This work was supported in part by the National Natural Science Foundation of China under Grant 51677162 and in part by the Natural Science Foundation of Hebei Province under Grant E2017203235. Recommended for publication by Associate Editor S. Golestan. *(Corresponding author: Liqiao Wang.)*

The authors are with the Key Laboratory of Power Electronics for Energy Conversion and Motor Drive of Hebei Province, Department of Electrical Engineering, Yanshan University, Qinhuangdao 066004, China (e-mail: brent@ysu.edu.cn; dqxb@stumail.ysu.edu.cn; samuelxopo@stumail.edu.cn; lizong@stumail.ysu.edu.cn).

Color versions of one or more figures in this article are available at https://doi.org/10.1109/TPEL.2025.3605048.

Digital Object Identifier 10.1109/TPEL.2025.3605048

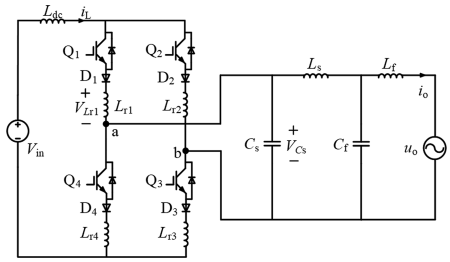

Fig. 1. Topology structure of single-phase CSI.

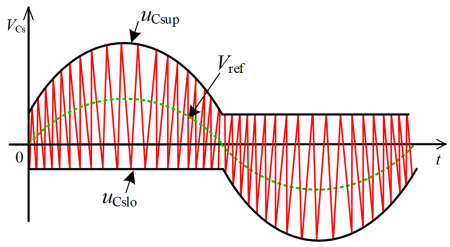

Fig. 2. Principle diagram of boundary voltage control.

the dc side directly affects the output on the ac side. In fact, in addition to the fixed frequency SPWM modulation method, there are also variable frequency control methods such as hysteresis modulation. Hysteresis modulation is a modulation strategy that determines whether a switch is turned ON or OFF by comparing the difference between a given signal and an actual signal with the hysteresis loop width. This control method samples and compares the ac side power without any specific requirements for dc side ripple. It does not require prediction or detection of dc side ripple. Therefore, it can be inferred that this control method may potentially reduce the required dc side inductance.

At present, hysteresis modulation methods have been widely studied in voltage source inverters. In [11], [12], and [13], they all adopt boundary current mode based on hysteresis modulation. In [14], based on the principle of hysteresis modulation, three different current control modes are proposed: boundary current mode (BCM); constant hysteresis current mode (CHCM); and variable hysteresis current mode (VHCM). During the operation of this control method, the ac side inductor current of the inverter is controlled to zero and then reverse flow occurs. At this point, resonance occurs between the ac inductance and the capacitance at both ends of the switching device, which enables zero voltage switching [15], [16].

According to the principle of duality, the idea of controlling the boundary current in a voltage source inverter to achieve soft switching can be transplanted to CSI. When it comes to soft switching of current source converters, current research is relatively scarce. One method is to add resonant components and auxiliary switching devices between the dc side and the inverter bridge to achieve soft switching [17], [18]. However, adding auxiliary circuits will lead to increased costs and volume, as well as increased control complexity. Another method is to achieve soft switching through modulation. In [19], no auxiliary circuit is required, and a pure control algorithm is used to make the soon to be turned ON switch withstand forward voltage, while the soon to be turned OFF switch withstand reverse voltage. But, this is a fixed frequency strategy, and the circuit parameters are also fixed, so it has not achieved full-range soft-switching. There must be hard switching near the phase switching point, and the control is also relatively complex. Due to the difficulty in modifying hardware parameters online, in order to achieve full-range soft-switching, a variable frequency control method can be used, which is the boundary voltage control (BVC) strategy proposed based on the duality principle mentioned above, and it does not require the addition of auxiliary circuits when implementing soft switching. ZCS can be achieved through resonance and the control is not complicated.

In this article, a BVC strategy suitable for CSI is proposed, which can not only reduce the value of dc side inductance, but also achieve ZCS. In addition, this method is suitable for applications involving new energy sources such as photovoltaic power generation, fuel cells, and hydrogen batteries, where the input voltage is relatively low and has a wide range of variations. By adopting this method, efficiency can be significantly improved and it has a promising prospect in the application of new energy. Finally, the correctness of the theoretical analysis is verified through simulation and experiments.

II. Boundary Voltage Control and Soft Switching Analysis

A. Topology Structure of Single-Phase CSI

The topology structure of the single-phase CSI used in this article is shown in Fig. 1. In the figure, $V_{\rm in}$ is the dc power supply, u_0 is the grid voltage, $Q_1{\sim}Q_4$ is the power switching device, $D_1{\sim}D_4$ is the forward series diode, $L_{\rm dc}$ is the dc side inductor, $L_{r1}{\sim}L_{r4}$ is the resonant inductor, C_s is the resonant capacitor, $L_{\rm s}$ and L_f are the filtering inductors, and C_f is the filtering capacitor.

B. Principle of Boundary Voltage Control

The BVC strategy adopted in this article is shown in Fig. 2, $u_{C\rm sup}$ and $u_{C\rm slo}$ are the upper and lower limits of BVC, the voltage V_{Cs} of resonant capacitor C_s is limited within the upper and lower boundary lines and changes like a sawtooth. $V_{\rm ref}$ is the given value of the BVC strategy obtained based on the output of the outer loop regulator. Structurally, $V_{\rm ref}$ corresponds to the fundamental component of the resonant capacitor voltage.

In BVC strategy, it is specified that the sine wave output reference voltage is determined by centerline of the upper and lower boundary lines. The upper boundary line is a sine wave with a dc component, while the lower boundary line is a fixed dc component V_B. These two boundary lines are located on both sides of the voltage zero axis reference line. Therefore, the centerline of the upper and lower boundary lines is the reference voltage for sine wave output, the expression can be given as

$$\begin{cases} u_{C\,\rm sup} = 2V_{\rm ref}\sin\omega t + V_B \\ u_{C\rm slo} = -V_B \end{cases} \quad (V_{\rm ref}\sin\omega t \geq 0)$$
$$\begin{cases} u_{C\,\rm sup} = V_B \\ u_{C\rm slo} = 2V_{\rm ref}\sin\omega t - V_B \end{cases} \quad (V_{\rm ref}\sin\omega t < 0)\,. \tag{1}$$

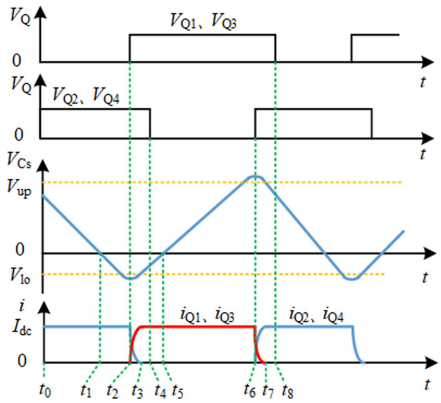

Fig. 3. Waveform diagram for implementing soft switch.

TABLE I
SWITCH STATUS SELECTION

$\mathrm{sgn}(V_{Cs})_{(k)}$	$Q_{1(k)}$	$Q_{3(k)}$	$Q_{2(k)}$	$Q_{4(k)}$
1	Off	Off	On	On
−1	On	On	Off	Off
$\mathrm{sgn}(V_{Cs})_{(k-1)}$	$Q_{1(k-1)}$	$Q_{3(k-1)}$	$Q_{2(k-1)}$	$Q_{4(k-1)}$

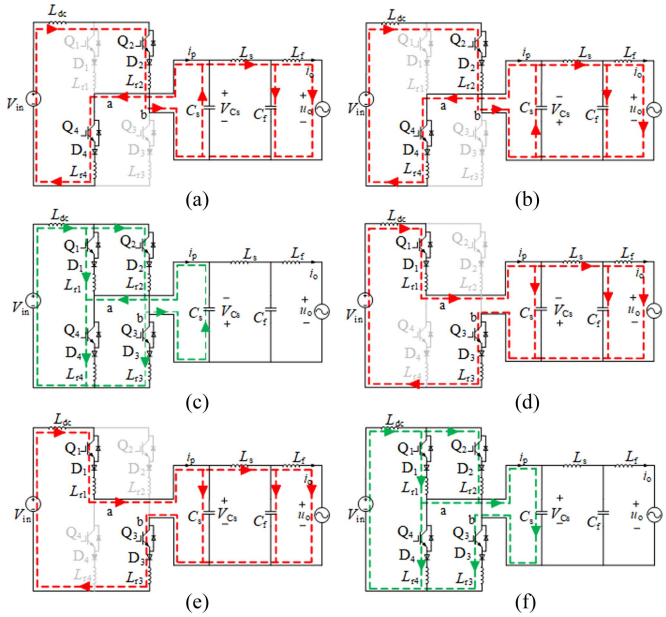

Fig. 4. Operating mode of the proposed topology. (a) Mode I. (b) Mode II. (c) Mode III. (d) Mode IV. (e) Mode V. (f) Mode VI.

C. Principle of Implementing Soft Switch

The switch conduction mode controlled by BVC can adopt bipolar mode or unipolar mode. In [20], research has found that when using unipolar mode, there is a sudden drop in the switching frequency of the high-frequency switching device to zero near the zero crossing point of the output current, causing the switching period to become infinite and resulting in distortion of the output waveform. During bipolar mode, there is no sudden drop to zero, and bipolar mode will make the output waveform smoother. To avoid the problem of zero crossing distortion, this article adopts bipolar mode.

The single-phase CSI proposed in this article adopts BVC and bipolar control. Due to the symmetry of the positive and negative half cycles, this article takes the positive half cycle as an example to analyze the principle of implementing ZCS achieved by BVC strategy. Assuming that the output current remains constant during the switching cycle. The driving signal of the switching device, the voltage of the resonant capacitor, and the current flowing through the switching device are shown in Fig. 3. The working state of the circuit can be divided into six parts within one switching cycle, as shown in Fig. 4.

The sign function of BVC is defined as $\mathrm{sgn}(V_{Cs})$, where V_{Cs} is the voltage across the resonant capacitor and can be expressed as

$$\mathrm{sgn}(V_{Cs})_{(k)} = \begin{cases} 1 & V_{Cs} > u_{C\sup} \\ \mathrm{sgn}(V_{Cs})_{(k-1)} & u_{C\mathrm{slo}} < V_{Cs} < u_{C\sup} \\ -1 & V_{Cs} < u_{C\mathrm{slo}} \end{cases}. \tag{2}$$

The BVC+bipolar control switch selection is given in Table I.

In a switching cycle, the state of switches in a circuit can be divided into two stages: steady conduction stage and overlapping conduction stage. During the time period of t_0-t_2 in Fig. 3, the switching devices Q_2 and Q_4 remain stably conductive, while Q_1 and Q_3 remain in an OFF state. At this point, the voltage of the resonant capacitor V_{Cs} begins to decrease, and the corresponding working states are shown in Fig. 4(a) and (b). Subsequently, during the time period of t_2-t_4 in Fig. 3, when the voltage of the resonant capacitor drops to the lower limit, the circuit enters the overlapping conduction stage. At this point, all four switches are conducting, and the circuit begins the commutation process, the working status is shown in Fig. 4(c). After the overlapping conduction stage is completed, during the time period of Fig. 3 t_4-t_6, the switching devices Q_1 and Q_3 are stably conducting, while Q_2 and Q_4 are turned OFF. The voltage of the resonant capacitor continues to rise, and the working state is shown in Fig. 4(d) and (e). Finally, during the time period of Fig. 3 t_6-t_8, when the voltage of the resonant capacitor rises to the upper boundary, the circuit enters the overlapping conduction stage again for commutation, and the working state at this time is shown in Fig. 4(f).

To achieve ZCS, it is required that the circuit completes the commutation process within the overlapping conduction time. During the overlapping conduction time, all four switches are conducting, where t_2-t_4 and t_6-t_8 represent the overlapping conduction time of the circuit, while t_2-t_3 and t_6-t_7 represent the commutation time. During the commutation time, series resonance occurs between the inductance connected in series with switching device and resonant capacitor. Transfer the current from the inductance on one bridge arm to the inductance on the other bridge arm to complete the circuit commutation. As shown in Fig. 4(c) and (f), in order to reduce the current flowing through the switching device to zero before the switch is turned OFF, the commutation time of the circuit needs to be less than the overlapping conduction time. Therefore, in order to achieve

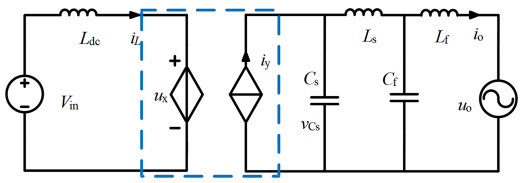

Fig. 5. Two port equivalent model of single-phase CSI.

ZCS, it is necessary to ensure that the commutation time of the circuit is less than the overlapping conduction time.

III. Analysis of Lightweight Inductance

A. Principle of Generating Second Harmonic Ripple of DC Side Inductor Current Under Traditional Modulation

The two port equivalent model of the single-phase CSI used in this article is shown in Fig. 5. The dc side voltage equation can be expressed as

$$V_{\text{in}} = L_{\text{dc}} \cdot \frac{di_L(t)}{dt} + u_x. \tag{3}$$

According to the two port power conservation theorem, it can be concluded that

$$i_L(t) \cdot u_x(t) = i_y(t) \cdot V_{Cs}(t). \tag{4}$$

The dc side inductor current is constantly changing over time and can be represented by the sum of the dc component i_{L_dc} and the ac component i_{L_ac}, which can be expressed as

$$i_L(t) = i_{L\_\text{dc}} + i_{L\_\text{ac}}(t). \tag{5}$$

Ignoring the influence of high-frequency components, the output current of the equivalent two port network and the voltage across the capacitor C_s can be given as

$$i_y(t) = i_L(t) \cdot \alpha \cdot \sin(\omega t) \tag{6}$$

$$V_{Cs}(t) = u_o(t) = U_o \cdot \sin(\omega t). \tag{7}$$

Combining with (3)–(7) and integrating them, it can be concluded that

$$i_{L\_\text{ac}}(t) = \frac{2V_{\text{in}} - \alpha \cdot U_o}{2L_{\text{dc}}} \cdot t + \frac{\alpha \cdot U_o}{4\omega \cdot L_{\text{dc}}} \cdot \sin(2\omega t). \tag{8}$$

Since i_{L_ac} is an ac current, taking the dc component as zero, it can be concluded that the modulation index α is

$$\alpha = \frac{2 \cdot V_{\text{in}}}{U_o}. \tag{9}$$

Combining (5), (8), and (9), it can be concluded that

$$i_L(t) = i_{L\_\text{dc}} + \frac{V_{\text{in}}}{2\omega \cdot L_{\text{dc}}} \cdot \sin(2\omega t). \tag{10}$$

The expression for the equivalent output current of a two ports network can be obtained as

$$\begin{cases} i_o(t) = i_{L\_\text{dc}} \cdot \alpha \cdot \sin(\omega t) + \frac{K}{2}(\cos(\omega t) - \cos(3\omega t)) \\ K = \frac{\alpha \cdot U_o}{4\omega \cdot L_{\text{dc}}} \\ \alpha = \frac{2 \cdot V_{\text{in}}}{U_o} \end{cases}. \tag{11}$$

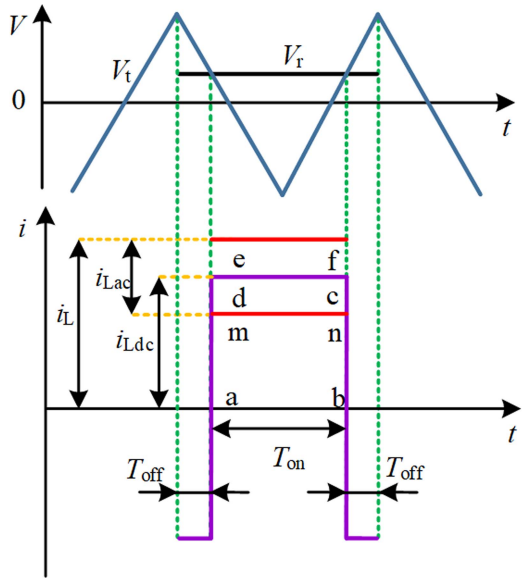

Fig. 6. Traditional SPWM modulation bipolar control.

When the single-phase CSI adopts traditional SPWM modulation, taking bipolar modulation as an example, its principle is shown in Fig. 6. According to the principle of area equivalence, it can be concluded that

$$\frac{i_o(t) \cdot \sin(\omega t) + i_L(t)}{2i_L(t)} = \frac{t_{\text{on}}}{T_s}. \tag{12}$$

Therefore, it can be concluded that

$$t_{\text{on}} = \frac{i_o(t) \cdot \sin(\omega t) + i_L(t)}{2i_L(t)} \cdot T_s. \tag{13}$$

For traditional SPWM modulation, based on the principle of area equivalence, it can be concluded that

$$i_o(t) = \frac{i_L(t) \cdot t_{\text{on}} - i_L(t) \cdot t_{\text{off}}}{T_s} = 2(d(t) - 1) \cdot i_L(t). \tag{14}$$

The single-phase CSI adopts traditional SPWM modulation, and the basic principle is to maintain a constant dc side current. When a single-phase CSI adopts traditional SPWM modulation, the basic principle is to maintain a constant dc side current. However, in reality, the dc side inductor current contains a second harmonic ac component. This leads to a difference between the actual current waveform and the ideal current waveform. Therefore, as shown in Fig. 6, the ideal area S_{abcd} enclosed by the current waveform and the time axis becomes *Sabef* or S_{abmn} in practice. Due to the fixed switching frequency, the turn ON and turn OFF times of the switch cannot be adjusted with changes in the dc side inductor current. Therefore, when the inductance current on the dc side is not constant, the principle of area equivalence will no longer apply, which will result in the appearance of third harmonic components in the output current of the inverter. According to (10) and (11), the amplitude of the second harmonic ripple component of the dc side inductor current and the amplitude of the third harmonic of the output current are inversely proportional to the dc side inductor value.

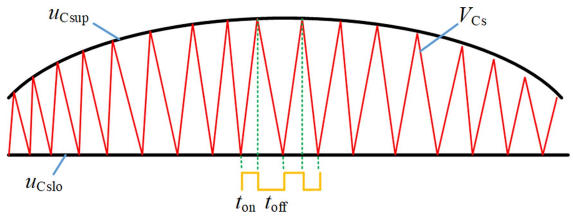

Fig. 7. Schematic diagram of BVC switch.

Therefore, directly reducing the inductance value on the dc side will lead to an increase in the third harmonic content of the output measured current, resulting in a decrease in output quality. So in order to achieve static area equivalence, single-phase CSI typically require larger inductance when using traditional SPWM modulation.

B. Analysis of the Principle of Reducing Inductance

The schematic diagram of BVC for switching ON or OFF is shown in Fig. 7. In bipolar control, taking the positive half cycle of the output voltage as an example, assuming that the dc side inductor current is a constant value and ignoring the shunt effect of the ac side filtering capacitor, it can be concluded that

$$\begin{cases} t_{\text{on}} = C_s \frac{u_{C\sup} - u_{C\text{slo}}}{i_L(t) - i_o(t)} \\ t_{\text{off}} = C_s \frac{u_{C\sup} - u_{C\text{slo}}}{i_L(t) + i_o(t)} \\ T_s = C_s \frac{(u_{C\sup} - u_{C\text{slo}}) \cdot 2 \cdot i_L(t)}{(i_L(t) + i_o(t)) \cdot (i_L(t) - i_o(t))} \end{cases}. \tag{15}$$

When the single-phase CSI adopts BVC and bipolar control, combined with formulas (1) and (15), it can be concluded that

$$\begin{cases} t_{\text{on}} = C_s \frac{2V_{\text{ref}} \sin \omega t + 2V_B}{i_L(t) - i_o(t)} \\ t_{\text{off}} = C_s \frac{2V_{\text{ref}} \sin \omega t + 2V_B}{i_L(t) + i_o(t)} \\ T_s = 4C_s \cdot i_L(t) \cdot \frac{V_{\text{ref}} \sin \omega t + V_B}{{i_L}^2(t) - {i_o}^2(t)} \end{cases}. \tag{16}$$

When using BVC strategy, the system can dynamically adjust the t_{on}, t_{off}, and T_s of the switching device based on the fluctuation between the dc side inductor current and the ideal value to maintain overall area equivalence. According to equation (16), when $i_L(t)$ is greater than i_{L_dc}, t_{on}, t_{off}, and T_s will dynamically decrease; On the contrary, when $i_L(t)$ is less than i_{L_dc}, these parameters will dynamically increase. This dynamic adjustment mechanism means that even if $i_L(t)$ changes, the system can adapt by adjusting t_{on}, t_{off}, and T_s. Therefore, it is not required that the dc side inductor current be a constant value, and only needs to fluctuate within a certain range. Therefore, the requirement for dc side inductor current ripple in BVC strategy is relatively low, which can reduce the value of the dc side inductor, help achieve inductor lightweighting, and improve the power density of the system.

The dc side inductance value cannot be too small, as the current of the dc side inductance contains second harmonic pulsation. Therefore, it can be concluded that

$$I_{L\_\max} + I_{L\_\min} = 2i_{L\_\text{dc}}. \tag{17}$$

Defining inductor current ripple as

$$\delta = \frac{i_{L\_\max} - i_{L\_\min}}{2i_{L\_\text{dc}}}. \tag{18}$$

Based on the relationship between inductive energy storage and current ripple, it can be concluded that

$$L_{\text{dc}} = \frac{V_{\text{in}}}{2 \cdot \delta \cdot \omega \cdot i_{L\_\text{dc}}}. \tag{19}$$

In the above equation, $\omega = 2\pi \cdot f$, $f = 100$ Hz. According to (19), the minimum value of the dc side inductance can be selected based on the input current ripple, input current, and input voltage of the circuit.

IV. Selection of Parameters

A. Resonant Inductor Design

According to the previous analysis, in order to achieve ZCS, the condition that the overlapping conduction time is greater than the commutation time must be met. During the commutation period, the voltage on each resonant inductor is $V_{Cs}/2$. When the voltage across the resonant capacitor drops to the lower boundary, the commutation voltage is at its minimum, which is $V_{Cs} = V_B$. The overlapping conduction time should be greater than the commutation time at this time

$$t_d > L_r \cdot \frac{2i_L(t)}{V_B}. \tag{20}$$

The stack times sampled in this article is $t_d = 2$ μs, $V_B = 35$ V, according to (20), $L_{r1\sim r4} < 2.33$ μH can be obtained. The final resonant inductor used in this article is 1 μH.

B. Resonant Capacitor Design

According to (16), the expression for the switching frequency can be obtained, as shown in

$$f_s = \frac{{i_L}^2(t) - {i_o}^2(t)\sin^2\omega t}{C_s \cdot 2V_B \cdot 2i_L(t)}. \tag{21}$$

When the output current is zero, considering the extreme case, when the current ripple is 30%, and when $I_{L\_\max} = 1.3i_L(t)$, the switching frequency reaches the maximum value within one switching cycle

$$f_{s\_\max} = \frac{1.3i_{L\_\text{dc}}}{4C_s \cdot V_B}. \tag{22}$$

This article assumes $V_B = 35$ V, $f_{s\_\max} = 50$ kHz, and selects the resonant capacitance value of 2 μF according to (22).

C. Filter Inductor and Capacitor Design

The ac side filter used in this article is an *LCL* filter. *LCL* filter is a commonly used filter in circuits, so its design process is not elaborated here. The *LCL* filter parameters selected in this article are: filter inductance L_s takes 5 mH, filter inductance L_f takes 1 mH, and filter capacitor C_f is 10 μF.

V. Design of Grid-Connected Control System

The topology of this article has been designed for a grid-connected control system, and its control strategy is shown in

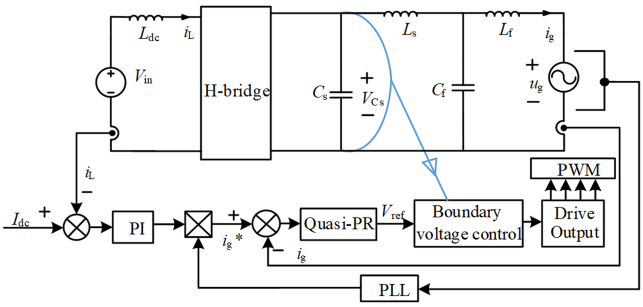

Fig. 8. Grid control strategy.

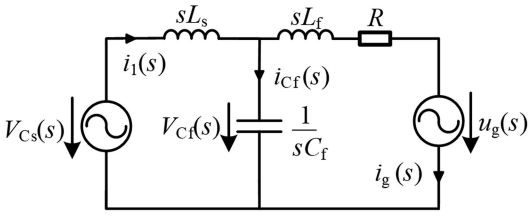

Fig. 9. Simplified circuit diagram.

Fig. 8. This strategy includes three control loops: the outer loop is the dc side inductor current loop, the middle loop is the ac side output current loop, and the inner loop is the BVC loop.

In the grid-connected control structure diagram, the difference is taken between the reference value and the sampled value of the dc side inductor current. The obtained difference is processed by a proportional integral (PI) controller, which adjusts the value to generate the reference amplitude of the c side output current. Then multiply it with the unit sine wave to obtain the given value of the output current on the ac side, where the unit sine wave is obtained by phase locking the grid voltage. Then, the given value of the output current on the ac side is subtracted from the sampled value, and the difference obtained is adjusted by a quasi-proportional resonant (PR) regulator to obtain the sine boundary line for BVC. Finally, the voltage across the resonant capacitor is limited between the set upper and lower boundary lines to obtain the driving signal for controlling the ON and OFF of the switching device.

When the inverter is connected to the grid, the voltage across the resonant capacitor is also used as the input signal for the *LCL* filter. The simplified circuit diagram of the filter at this time is shown in Fig. 9, where R is the equivalent resistance on the grid-connected ac side.

By analyzing Fig. 9 in the frequency domain, it can be concluded that

$$\begin{cases} i_1(s) = \frac{1}{sL_s}\left(V_{Cs}(s) - V_{Cf}(s)\right) \\ V_{Cf}(s) = \frac{1}{sC_f}\left(i_1(s) - i_g(s)\right) \\ i_g(s) = \frac{1}{sL_f+R}\left(V_{Cf}(s) - u_g(s)\right) \end{cases}. \tag{23}$$

According to (23), the control structure diagram of the intermediate loop for grid-connected current can be drawn as shown in Fig. 10.

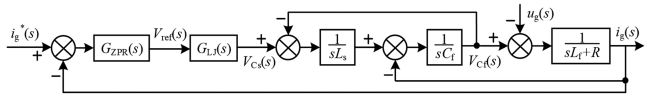

Fig. 10. Structure diagram of grid-connected current loop.

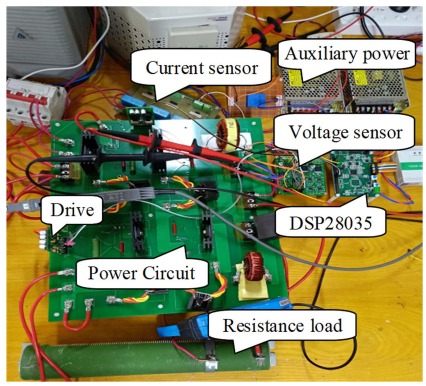

Fig. 11. Experimental prototype.

For the convenience of analysis, the boundary voltage loop can be equivalent to a first-order inertia link, and its closed-loop transfer function can be written as

$$G_{LJ}(s) = \frac{V_{Cs}(s)}{V_{\text{ref}}(s)} = \frac{1}{C_s s + 1}. \tag{24}$$

The output current loop on the ac side compares the given value with the sampled value, and through the regulating effect of the regulator, it is required to achieve zero static error tracking of the sine ac difference signal. To meet this requirement, a quasi-PR regulator is selected for regulation, and the transfer function of the quasi-PR regulator is

$$G_{\text{ZPR}}(s) = K_p + \frac{2K_r\omega_c s}{s^2 + 2\omega_c s + \omega_0^2}. \tag{25}$$

In the formula, K_p and K_r represent the ratio and resonance parameter of the PR regulator, respectively; ω_0 is the fundamental angular frequency; and ω_c is used to adjust the gain bandwidth of the quasi-PR regulator at the resonance point.

VI. Experiment Validation

The control method in this article adopts a new hybrid chip TMS320F28035 that can achieve digital analog hybrid control, and its control complexity is comparable to SPWM modulation. The maximum switching frequency set in this article is 50 kHz, and the upper limit of the V_{Cs} design frequency matches it. The enhanced isolation amplifier ISO224 used for sampling in this article has an output bandwidth of 275 kHz, and the digital analog hybrid chip can handle switching frequencies above 100 kHz, both of which meet the requirements of sampling and control.

In order to verify the correctness of the theoretical analysis in the previous text, an experimental platform is built in this article, as shown in Fig. 11, and the experimental parameters are given in Table II.

TABLE II
EXPERIMENTAL PARAMETERS

Parameters	Value
Q_1-Q_4	IKW40N120CS6XKSA1
D_1-D_4	VS-E5PH6012L-N3
V_{in}	30 V
$L_{r1\sim4}$	1 μH
L_s	5 mH
C_f	10 μF
V_g	110 V
C_s	2 μF
L_f	1 mH
R_L	40 Ω

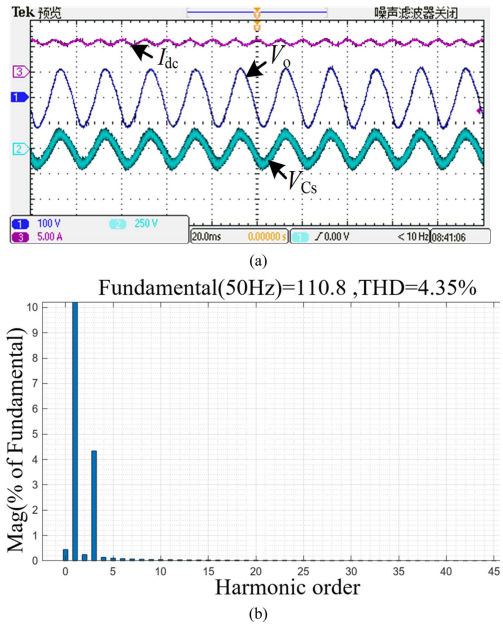

Fig. 12. Traditional modulation of large inductance experimental waveform. (a) Experimental waveform. (b) FFT analysis of output voltage.

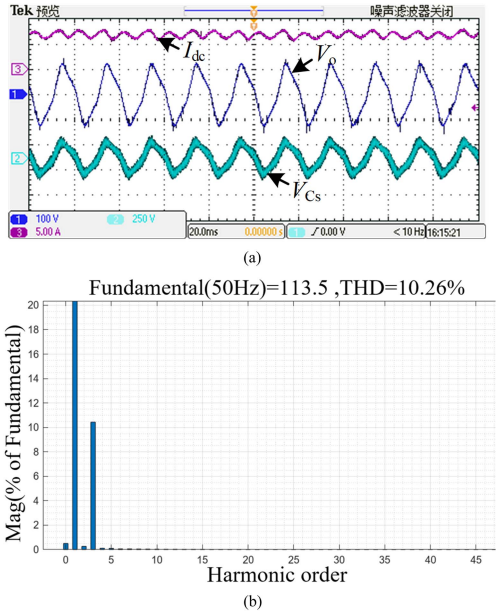

Fig. 13. Traditional modulation small inductance experimental waveform. (a) Experimental waveform. (b) FFT analysis of output voltage.

A. *Analysis of Inductance Reduction Experiment*

The experimental setting of the dc side inductor current in this article is 6 A. A comparative experiment is conducted between single-phase CSI using a 25 mH large inductor and a 10mH inductor under traditional SPWM modulation, and single-phase CSI using a 10 mH inductor under BVC. Figs. 12 and 13 show the experimental output waveforms using a 25 mH large inductor and a 10 mH inductor, respectively, under traditional SPWM control.

From Fig. 12(a), it can be seen that due to the use of a 25 mH large inductor on the dc side, the second harmonic ripple of the inductor current on the dc side is effectively suppressed, and the ripple of the inductor current is 12%. From Fig. 12(b), it can be seen that the third harmonic content of the output voltage is relatively low.

When the dc side inductance value is reduced to 10 mH, it can be clearly seen from Fig. 13(a) that the second harmonic ripple component of the inductance current increases significantly compared to Fig. 12(a), and the inductance current ripple reaches 27%. Comparing Figs. 12 and 13, it can be clearly seen that under traditional SPWM modulation, directly reducing the dc side inductance value will lead to a significant decrease in the quality of the output voltage waveform, with total harmonic distortion (THD) increasing from 4.35% to 10.26%, and the third harmonic content of the output voltage significantly increasing. This is because under traditional SPWM control, directly reducing the inductance value will cause an increase in the second harmonic ripple component of the dc side inductance current, which in turn leads to an increase in the third harmonic content on the output side. The experimental results are consistent with the theoretical analysis in the following section.

Ensure that all other parameters remain unchanged, and under BVC, the experimental waveform of single-phase CSI with a 10 mH dc side inductor is shown in Fig. 14. From Fig. 14(a), it can be seen that due to the small inductance value on the dc side, the current ripple of the dc side inductance is 26%. However, as shown in Fig. 14(b), it can be seen that the quality of the output voltage waveform has significantly improved, and the THD is 2.34%, which meets the requirements of IEEE Std 519-2014 [21]. In addition the third harmonic content on the output side is lower, which is less than the experimental results obtained using 25 mH and 10 mH inductors under SPWM modulation, as shown in Figs. 12 and 13, respectively. This results in better output quality on the ac side.

Based on the comprehensive analysis of Figs. 12, 13, and 14, it can be concluded that BVC strategy can reduce the dc side inductance value of single-phase current type inverters. The experimental results are consistent with the theoretical analysis in the previous section.

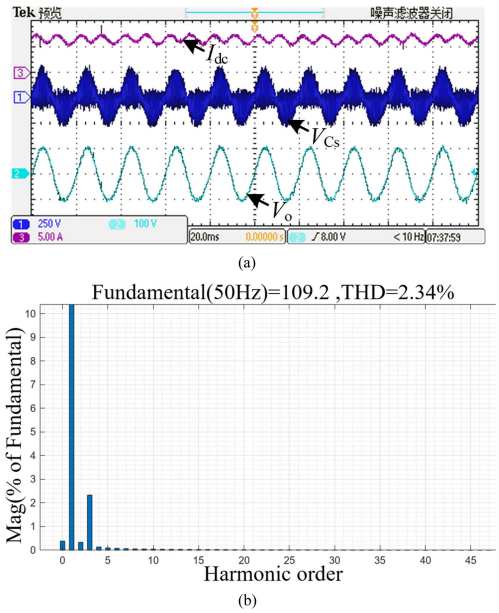

Fig. 14. Experimental waveform of small inductance controlled by boundary voltage. (a) Experimental waveform. (b) FFT analysis of output voltage.

B. Experimental Analysis of Soft Switch and Load Disturbance

The four high-frequency switching devices in this topology work similarly. Due to space limitations, taking switching device Q_1 as an example for analysis, and the relevant waveform diagram is shown in Fig. 15.

From Fig. 15, it can be seen that Q_1 only turns OFF after the current flowing through it drops to zero, achieving ZCS. The experimental results are consistent with the theoretical analysis presented earlier.

Keeping the input voltage $V_{\text{in}} = 30$ V and the peak output voltage at 110 V, the load suddenly increases from half load to full load. The experimental waveform is shown in Fig. 16(a). In addition, keeping the parameters unchanged, the load suddenly dropped from full load to half load, and the experimental waveform is shown in Fig. 16(b). It can be seen that the inverter can effectively resist load interference. On the one hand, when the disturbance is added, the output current only has a slight fluctuation, but can quickly return to steady state, and the waveform quality is good. On the other hand, when the load disturbance occurs, the peak value of the output voltage is doubled or reduced.

C. Grid-connected Experimental Analysis

In order to verify the grid-connected capability of the proposed inverter, the grid-connected experiment is carried out. The inherent THD of the grid voltage is 8.3%. The grid-connected experiment is set with a grid-connected current amplitude of 3 A and a grid-connected voltage amplitude of 110 V. The experimental waveform is shown in Fig. 17. From Fig. 17, it can be seen that the grid-connected current is of the same frequency and phase as the grid voltage, and all harmonics meet the requirements for grid connection. The inverter in this article

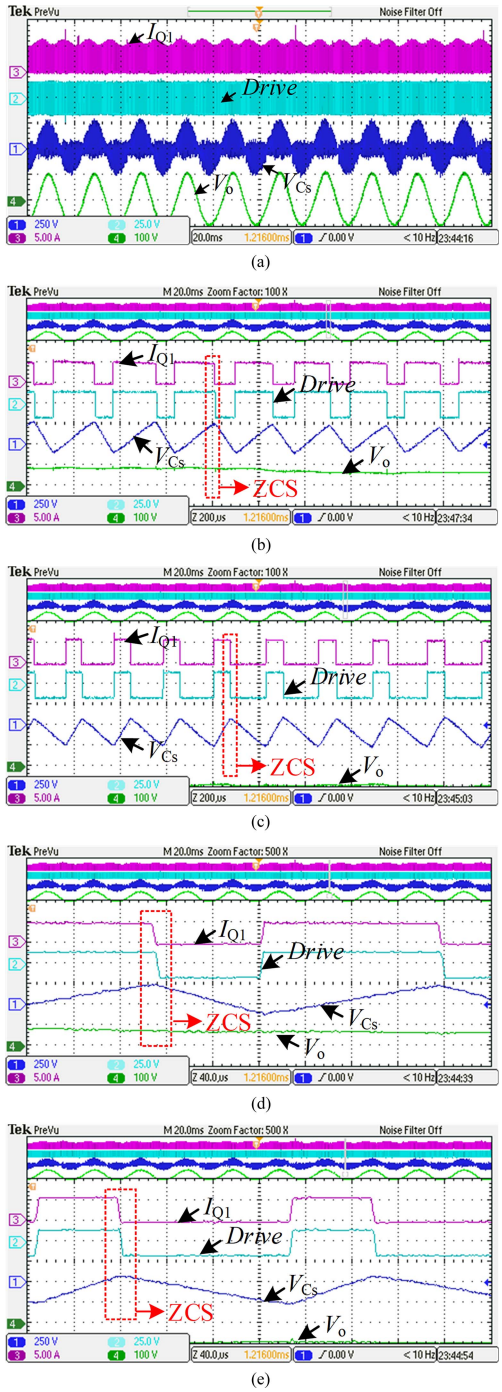

Fig. 15. Implement relevant waveforms for soft switching. (a) Related waveforms and output voltage waveforms of switch Q_1. (b) Positive half cycle ZCS waveform. (c) Negative half cycle ZCS waveform. (d) Positive half cycle ZCS waveform. (e) Negative half cycle ZCS waveform.

is suitable for low-power single-phase photovoltaic systems. Through the analysis of FFT in Fig. 17, as given in Table III, the magnitude of harmonic current meets the relevant requirements of class A equipment in IEC 61000-3-2 standard [22].

Maintain the peak voltage of the power grid at 110 V (78 V rms) and input voltage $V_{\text{in}} = 30$ V. The waveforms of the given current suddenly increasing from 6 to 10 A and suddenly

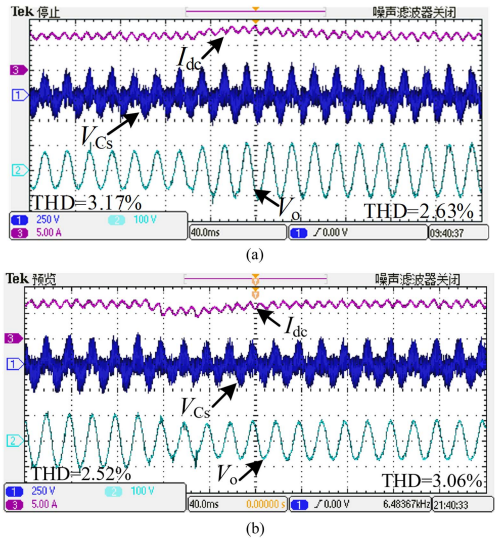

Fig. 16. Waveform of load disturbance. (a) Half load to full load. (b) Full load to half load.

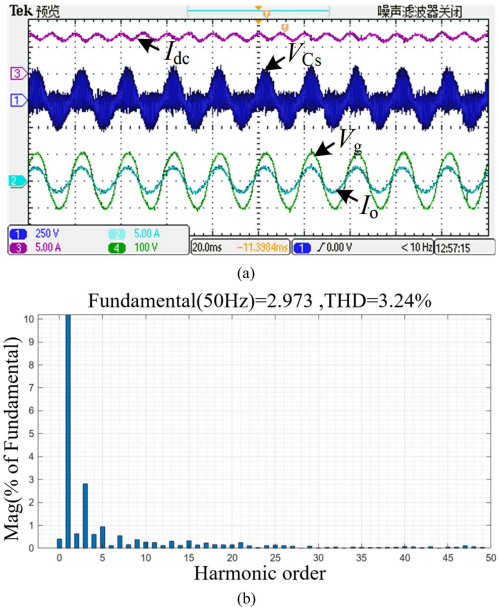

Fig. 17. Grid-connected experimental waveform. (a) Voltage and current waveform. (b) FFT analysis of grid-connected current.

decreasing from 10 to 6 A are shown in Fig. 18(a) and (b), respectively. It can be seen that when the given current suddenly changes, there will be fluctuations in the ac measured current, but it will soon stabilize again and the inverter can still operate normally.

D. Losses and Efficiency Analysis

The efficiency measured in the experiment is shown in Fig. 19. The peak efficiency occurs between 140 and 200 W, and as the output power increases, the efficiency first increases and then decreases, with a peak efficiency of about 91.3%. Fig. 20 shows the comparison of power losses under SPWM and BVC. It can

TABLE III
COMPARISON OF HARMONIC CURRENT

Harmonic Order	Specified Limit/A	Test Value/A	Requirement Met
2	1.08	0.018	yes
3	2.30	0.087	yes
4	0.43	0.019	yes
5	1.14	0.029	yes
6	0.3	0.003	yes
7	0.77	0.015	yes
8	0.23	0.006	yes
9	0.40	0.012	yes
10	0.184	0.0078	yes
11	0.33	0.009	yes
12	0.153	0.0036	yes
13	0.21	0.011	yes
14	0.131	0.0042	yes
15	0.15	0.0105	yes
16	0.115	0.0045	yes
17	0.132	0.0063	yes
18	0.102	0.006	yes
19	0.118	0.0057	yes
20	0.092	0.0057	yes
21	0.107	0.0063	yes
22	0.084	0.003	yes
23	0.098	0.0015	yes

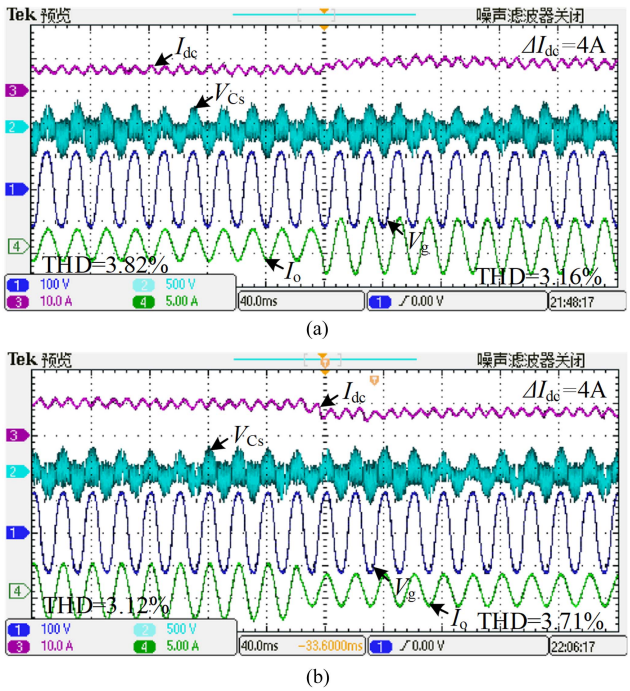

Fig. 18. Waveform of given current disturbance. (a) Sudden increase of given current. (b) Sudden drop of given current.

be seen that as the frequency increases, the losses under both SPWM and BVC will increase. However, BVC achieves ZCS, and compared to the hard switch under SPWM control, the power loss of BVC is smaller.

In this article, the focus is on soft switching and reducing inductance. ZCS can improve the efficiency of switching devices.

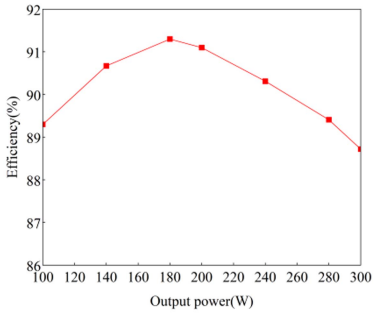

Fig. 19. Measured efficiency.

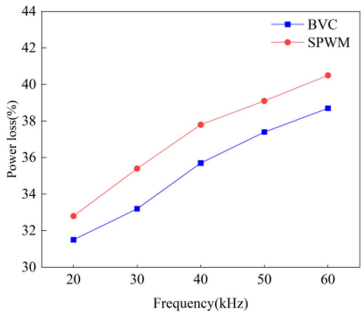

Fig. 20. Comparison of power loss between SPWM and BVC.

For the part of reducing inductance, strict design is not carried out from the perspective of efficiency, but ready-made inductors are directly purchased for experimentation. In fact, from the perspective of efficiency, redesigning inductors is expected to further improve the efficiency of circuits.

The experimental results listed in this article are obtained under low voltage and low-power conditions. When expanding to higher voltage and larger capacity conditions, it is necessary to discuss the stress of the switching devices; and also need to discuss passive components, especially the issue of inductance value on the dc side. As a single-phase grid-connected current-source inverter, its application is supposed to be in low-voltage distribution grid, and its voltage level is usually 110 V or 220 V, while the grid side voltage level in this prototype is 110 V. Therefore, for the voltage stress of the device, the experimental results provided in this article are sufficiently reliable. For current stress, since the power capacity of single-phase inverters usually does not exceed 10 kW, calculated based on a grid side voltage of 110 V, the value of grid side current is 90 A, which is not a very high. Therefore, when it is necessary to increase the power capacity, from the perspective of switching devices, only the driving and interference problems caused by larger currents need to be considered, which is not a difficult problem for a 10 kW device.

According to (19), under the condition of constant dc voltage, the larger the current, the greater the power, which will result in a smaller inductance value. That is to say, from the perspective of reducing inductance value, the higher the power, the greater the decrease in inductance value. Of course, although the inductance value decreases, its current increases, so its volume change is not significant. But, it is much smaller than the inductance under SPWM modulation at the same current level. In short, from the perspective of reducing the inductance value, increasing power capacity is not a big problem.

VII. Discussion on Weak Grid Scenarios

In this article, the BVC strategy is a closed-loop control strategy under strong grid conditions and is an effective method for achieving ZCS. Under weak grid conditions, its impedance characteristics are different from those of strong grid, and are related to grid structure and transmission line distance, so the performance of inverters may be affected. However, from the perspective of ZCS, the BVC used in this article is a tracking control strategy that achieves ZCS by tracking a given voltage. The implementation of ZCS is related to the period of resonance caused by the inductance and capacitance connected with the switching device, the turn OFF time of the switching device, and the commutation time. It is determined by the capacity of the system and the characteristics of the devices, and is not related to the impedance of the power grid. Therefore, weak grid conditions do not affect the implementation of ZCS.

However, under weak grid conditions, fluctuations, distortions, phase shifts of the grid voltage, and the resulting decline in PLL performance may lead to inaccurate reference voltage V_{ref}, resulting in a decrease in actual control effectiveness. In fact, these problems can be solved by using more robust phase-locked loops, such as second order generalized integrator (SOGI) phase-locked loop (PLL). In addition, the filter in this inverter is designed according to the strong grid. Considering that the impedance on the transmission line on the grid side cannot be ignored in weak grid, and it does not have a constant value. When designed according to the above scheme, it may cause oscillation. Therefore, it is necessary to introduce some more robust control schemes, such as damping control schemes, feedforward control schemes, state feedback control schemes, etc. If necessary, online identification of grid impedance is also required. Through these measures, reliable and high-quality grid connected operation of inverters can be achieved under complex weak grid conditions, meeting practical application needs.

VIII. Conclusion

In this article, a BVC strategy is proposed and applied to single-phase CSI. The feasibility of this theory has been verified through experiments. Due to limited laboratory conditions, all results in this article are based on results are based on a low-power prototype. The research focuses on single-phase grid-connected inverter is studied, which has a limited power level, generally not exceeding 10 kW. As the power level increases, the current stress on the switch will increase. To improve its performance, the switching frequency can be further increased and new types of silicon carbide or gallium nitride devices can be used. Experimental results show that the BVC strategy can achieve ZCS of single-phase CSI and reduce circuit losses; And effectively reduce the inductance value on the dc side, reducing the size of the inverter.

REFERENCES

[1] B. Guo et al., "Optimization design and control of single-stage single-phase PV inverters for MPPT improvement," *IEEE Trans. Power Electron.*, vol. 35, no. 12, pp. 13000–13016, Dec. 2020.

[2] N. Tak and S. K. Chattopadhyay, "Two-stage three-phase transformerless hybrid multilevel inverter for solar PV application," *IEEE Trans. Ind. Electron.*, vol. 71, no. 6, pp. 5386–5398, Jun. 2024.

[3] L. Wang and X. Yang, "A single-stage common-ground inverter with high-voltage-gain ability," *IEEE Trans. Power Electron.*, vol. 40, no. 5, pp. 7058–7069, May 2025.

[4] M. Rajeev and V. Agarwal, "Single phase current source inverter with multiloop control for transformerless grid–PV interface," *IEEE Trans. Ind. Appl.*, vol. 54, no. 3, pp. 2416–2424, May/Jun. 2018.

[5] T.-D. Duong, M.-K. Nguyen, T.-T. Nguyen, H. Cha, Y.-C. Lim, and J.-H. Choi, "Switching-cell structure-based generic five-level current-source inverter," *IEEE Trans. Ind. Electron.*, vol. 70, no. 6, pp. 5696–5706, Jun. 2023.

[6] Y. Si et al., "A single-phase single-stage current source inverter with buck-boost capability and reduced inductor," *IEEE J. Emerg. Sel. Topics Power Electron.*, vol. 12, no. 4, pp. 3505–3515, Aug. 2024.

[7] S. T. Basabi and H. Farzanehfard, "Novel transistor-less series power decoupling in conventional current source inverter for PV application," in *Proc. 11th Power Electron., Drive Syst., Technol. Conf.*, Feb. 2020, pp. 1–5.

[8] M. A. Vitorino and M. B. D. R. Correa, "Compensation of DC link oscillation in single-phase VSI and CSI converters for photovoltaic grid connection," in *Proc. IEEE Energy Convers. Congr. Expo.*, Sep. 2011, pp. 2007–2014.

[9] M. A. Vitorino, M. B. R. Correa, and C. B. Jacobina, "Single-phase power compensation in a current source converter," in *Proc. IEEE Energy Convers. Congr. Expo.*, Sep. 2013, pp. 5288–5293.

[10] R. T. H. Li, H. S. Chung, and T. K. M. Chan, "An active modulation technique for single-phase grid-connected CSI," *IEEE Trans. Power Electron.*, vol. 22, no. 4, pp. 1373–1382, Jul. 2007.

[11] S. M. Tayebi, N. Kutkut, and I. Batarseh, "Analysis and optimization of BCM peak current mode control techniques for microinverters," in *Proc. IEEE Appl. Power Electron. Conf. Expo.*, Mar. 2017, pp. 2644–2651.

[12] G. Son, Z. Huang, Q. Li, and F. C. Lee, "Analysis and control of critical conduction mode high-frequency single-phase transformerless PV inverter," *IEEE Trans. Power Electron.*, vol. 36, no. 11, pp. 13188–13199, Nov. 2021.

[13] C. Marxgut, F. Krismer, D. Bortis, and J. W. Kolar, "Ultraflat interleaved triangular current mode (TCM) single-phase PFC rectifier," *IEEE Trans. Power Electron.*, vol. 29, no. 2, pp. 873–882, Feb. 2014.

[14] Q. Zhang, H. Hu, D. Zhang, X. Fang, Z. J. Shen, and I. Bartarseh, "A controlled-type ZVS technique without auxiliary components for the low power DC/AC inverter," *IEEE Trans. Power Electron.*, vol. 28, no. 7, pp. 3287–3296, Jul. 2013.

[15] Y. Tang, C. Zhang, Y. Guo, H. Sun, and L. Jiang, "Optimization of zero-crossing distortion for unipolar BCM grid-tied inverter," *IEEE J. Emerg. Sel. Topics Power Electron.*, vol. 11, no. 4, pp. 3680–3691, Aug. 2023.

[16] Z. Zhang, J. Zhang, S. Shao, and J. Zhang, "A high-efficiency single-phase T-type BCM microinverter," *IEEE Trans. Power Electron.*, vol. 34, no. 1, pp. 984–995, Jan. 2019.

[17] P. Cancelliere, V. D. Colli, R. Di Stefano, and F. Marignetti, "Modeling and control of a zero-current-switching DC/AC current-source inverter," *IEEE Trans. Ind. Electron.*, vol. 54, no. 4, pp. 2106–2119, Aug. 2007.

[18] Z. Wang, Y. Xu, P. Liu, Y. Zhang, and J. He, "Zero-voltage-switching current source inverter Fed PMSM drives with reduced EMI," *IEEE Trans. Power Electron.*, vol. 36, no. 1, pp. 761–771, Jan. 2021.

[19] Z. Bai, Z. Zhang, and X. Ruan, "A natural soft-commutation PWM scheme for current source converter and its logic implementation," *IEEE Trans. Ind. Electron.*, vol. 58, no. 7, pp. 2772–2779, Jul. 2011.

[20] T.-F. Wu, C.-L. Kuo, K.-H. Sun, and H.-C. Hsieh, "Combined unipolar and bipolar PWM for current distortion improvement during power compensation," *IEEE Trans. Power Electron.*, vol. 29, no. 4, pp. 1702–1709, Apr. 2014.

[21] *IEEE Recommended Practice and Requirements for Harmonic Control in Electric Power Systems*, IEEE Std 519–2014, Jun. 2014, pp. 1–29.

[22] IEC 61000-3-2, "Electromagnetic compatibility (EMC) – Part 3-2: Limits – limits for harmonic current emissions (equipment input current $\leq$16 A per phase)," International Electrotechnical Commission, 2020.

Liqiao Wang was born in Hebei Province, China, in 1974. He received the B.S. and M.S. degrees from Yanshan University, Qinhuangdao, China, in 1996 and 1999, respectively, and the Ph.D. degree from Zhejiang University, Hangzhou, China, in 2003, respectively, all in electrical engineering.

From 2005 to 2012, he was an Associate Professor with Yanshan University. Since 2012, he has been a Professor with the Department of Electrical Engineering, Yanshan University. His research interests include high-frequency power conversion, pulse modulation theory, large-power power electronic converter, renewable energy power generation, smart grid, and so on.

Dr. Wang is also a Senior Member of China Electrotechnical Society.

Zhaozhao Tang was born in Hebei Province, China in 2000. He received the B.S. degree in civil engineering in 2022 from Yanshan University, Qinhuangdao, China, where he is currently working toward the M.S. degree in electrical engineering.

His current research interests include grid-connected inverter, current-source rectifier, zero-current switching, and solar power generation.

Xiaoshan Xing was born in Hebei Province, China, in 1995. She received the B.S. degree in electrical engineering and automation and the M.S. degree in electrical engineering from Yanshan University, Qinhuangdao, China, in 2017 and 2023, respectively.

She is currently with Qingdao Sifang Alstom Railway Transportation Equipment Co., Ltd., Qingdao, China. Her current research interests include grid-connected inverter, variable-frequency modulation strategy.

Zong Li was born in Hebei Province, China, in 2000. He received the B.S. degree in electrical engineering and automation in 2022 from Yanshan University, Qinhuangdao, China, where he is currently working toward the M.S. degree in electrical engineering.

His current research interests include three-phase grid-connected inverter and three-phase voltage-source rectifier.